ME525 Applied Acoustics Lecture 13 Winter 2022 The Rayleigh integral, beam patterns, hydrodynamic and geometric near and far fields

Peter H. Dahl, University of Washington

Rayleigh integral

We have now studied the Helmholtz-Kirchhoff integral , Eq.(1), to compute the sound radiation from a surface S based on a generally variable normal velocity $u_n(\vec{r}_s)$ over the surface at position $\vec{r}_s$ plus a similarly varying pressure distribution $p(\vec{r}_s)$ which can depend in complicated way on $u_n(\vec{r}_s)$. (Where once again $p(\vec{r},t) = p(\vec{r})e^{-i\omega t}$.)

$$p(\vec{r}) = \int_S [p(\vec{r}_s)\frac{\partial g}{\partial n} - i\omega\rho_0 u_n(\vec{r}_s)g(\vec{r},\vec{r}_s)]dS \tag{1}$$

Solution of Eq.(1) poses difficult numerical challenges, primarily involving finding the unknown pressure distribution $p(\vec{r}_s)$. In some problems, such as sound radiation from a spherical source of fixed radius a, the relation between $p(\vec{r}_s)$ and $u_n(\vec{r}_s)$ is easily worked out and the integral solved exactly.

If there are situations where the first integral in Eq.(1) can be ignored, the solution is greatly simplified. Fortunately, this happens in many situations where the radiation surface S is planar (or at least approximately so), as was first demonstrated by Rayleigh (see Junger and Feit, 1993).

To understand how this happens we introduce the concept of a *baffle* where there is a limited portion of the planar surface that is vibrating and generating sound, with the remaining portion of the surface idealized as rigid. The baffle within which the aperture (or sound radiating part) is set (Fig. 1) theoretically extends to infinity in all directions and restricts the sound field to only one hemisphere but otherwise does not vibrate.

The boundary condition on the aperture is such that it is impenetrable to sound, and reflects sound completely. This means pressure on such a boundary will double (as if someone talking very close to a hard wall- try it yourself), rather than pressure going to zero as observed from sound below an air-water interface. The result of this reasoning is such that the first term of the Helmoltz-Kirchhoff equation is eliminated and the second term is increased by a factor of two (Pierce, 1989)

We now write formally the Rayleigh integral as

$$p(\vec{r}) = -i2\omega\rho_0 \int_S u_n(\vec{r}_s)g(\vec{r},\vec{r}_s)dS. \tag{2}$$

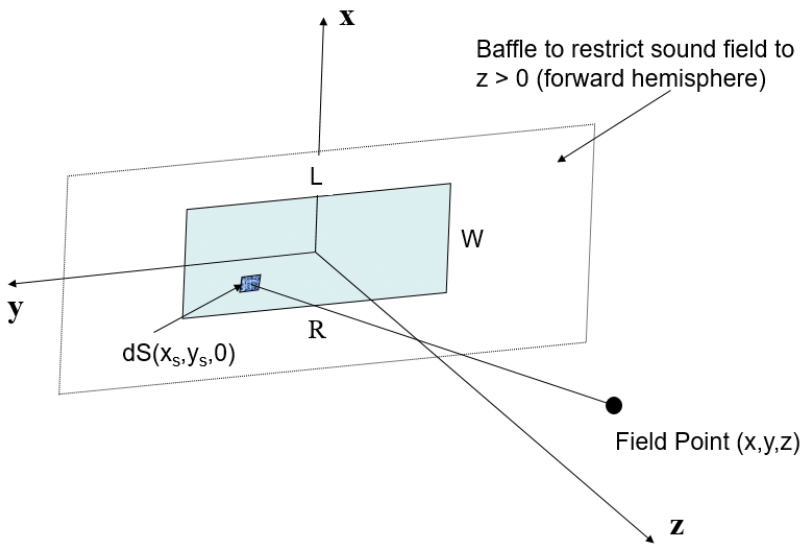

Figure 1: Cartesian coordinate system established at the center of radiating rectangular aperture confined by a baffle to restrict the sound field to $z > 0$. The elemental source dS is distance R from the field point where $R = \sqrt{(x - x_s)^2 + (y - y_s)^2 + z^2}$

For the planar geometries involved in evaluating the Rayleigh integral, a Cartesian coordinate system centered on the radiating aperture (Fig. 1) is best, where

$$p(\vec{r}) = \frac{-i\omega\rho_0}{2\pi} \int_S u_n(x_s, y_s) \frac{e^{ikR}}{R} dx_s dy_s \tag{3}$$

with $R = |\vec{r} - \vec{r}_s|$.

Next we relax the definition of a baffle that extends to infinity, and even relax (somewhat) the criterion that the aperture be perfectly flat. Figure 2 shows to planar-like radiating apertures and associated baffles that are used on autonomous underwater vehicles. (Notice these are slightly curved to match the hull shape of the AUV.) Furthermore knowing the characteristic length scales of aperture, as in L and W in Fig. 2, combined with sound frequency to give kW and kL will yield much information without having to lift a finger!

Additionally we often encounter situations that simplify the computation even further, such as case (Fig. 3) where $W < L$ and $kW << 1$, representing a line array. In these situations Eq. (3) is effectively a 1-D integral along the y-axis using dy_s, and dx_s can be considered a constant representing W.

Beam patterns

We use the Rayleigh integral to study the beam pattern for radiation from a disk of diameter D at particular frequency f and wavelength λ. A common result for this is Eq. (10) in the monograph entitled High Frequency Underwater Sound in your resource section on the website.

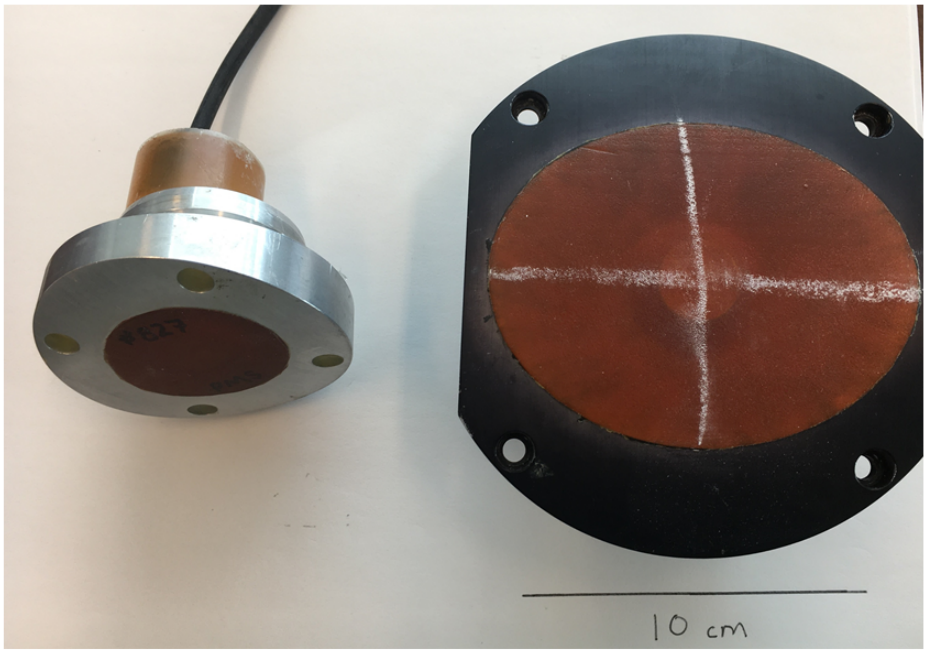

Figure 2: Two planar-like apertures. On the left an orange-colored aperture (made of acoustic transparent material) is surrounded by a baffle (black); chalk lines identify two characteristic length scales, say L and W of the aperture. On the right is smaller aperture surrounded by an metalic frame that serves the baffled. Both apertures and baffle are slightly curved to fit within the side of an autonomous underwater vehicle.

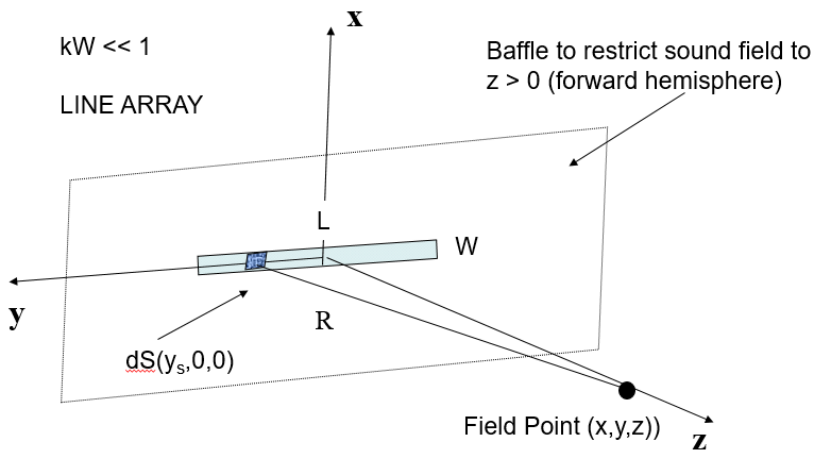

Figure 3: Cartesian coordinate system established at the center of radiating line aperture confined to a baffle to restrict the sound field to $z > 0$. The elemental source dS is distance R from the field point where $R = \sqrt{(y - y_s)^2 + x^2 + z^2}$. Because the aperture width is narrow in the sense of $kW << 1$ the aperture is considered a line array.

The problem studied is radiation from a disk of diameter 2 m, observed at a set of field points all at range 10 m from center of disk but at different angles. A top view [Fig. 4 (a)] shows field points in blue, all having $|\vec{r} - \vec{r}_s|$ equal to 10 m (coordinate axis centered on disk) but differing θ with respect to a line perpendicular to the disk center. another view is [Fig. 4 (b)] the disk looks solid red, but it is composed of 1200 points, each with elemental area dS, the sum of all elemental areas approximating the total area. Note: strictly speaking, a rigid baffle surrounds the radiating disk. However the baffle is just a convenient conceptual bridge to help justify use of the Rayleigh integral. For many applications as in this case, this feature of the problem can be effectively ignored. The key property is the basic flatness of the aperture.

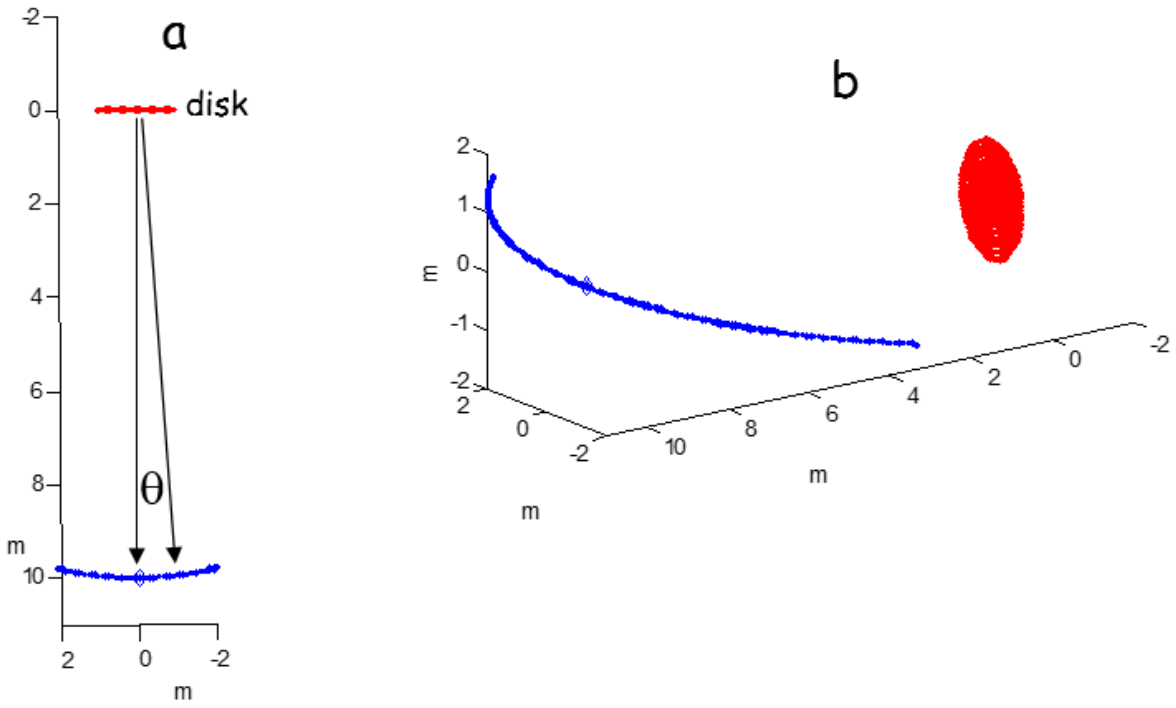

Figure 4: Problem studied: radiation from a disk of diameter 2 m, (a) observed at a set of field points (blue dots) all at range 10 m from center of disk but at different angles θ (b) alternate view showing the red disk and several field points at the same range but varying angle θ. Note that the set of field points align with a line that would divide the disk evenly.

To complete the numerical integral each dS is multiplied by $\frac{-i\omega\rho_0 u_n}{2\pi}\frac{e^{ikR}}{R}$, where R connects a particular dS to the field point, and where u_n is normal velocity on the disk. In many problems u_n is unknown, but can be assumed constant over the face of radiating aperture. Since the problem involves studying the pressure variation with angle and not the value of pressure *per se* it is therefore not essential to know u_n, which can be set to unity or to some notional value. The subject of the study, pressure variation versus angle and range, is completely embodied by the integral in Eq. (3).

Next define the pressure for $\theta = 0^\circ$ as the *on-axis* pressure as it (generally) will be maximal on the center axis where $\theta = 0^\circ$. Also for this simple disk problem the circular symmetry means angular dependence (called the beam pattern) can be characterized by one angle, θ; more complicated problems require two angles. Evaluate the computed pressure (or quantity proportional to it) from the Rayleigh integral and express results in decibels as follows

$$20 \log_{10}(|p(\theta)|/|p(\theta = 0^\circ)|) \tag{4}$$

where pressure is computed at fixed range but variable θ. Plotting Eq. (4) as a function of θ gives a *beam pattern*. One needs to know the beam pattern for design purposes that depend on application, e.g., a high-resolution narrow beam for detail versus broad beam.

Hydrodynamic near field versus Geometric near and far fields

In Lecture 6 the concept of a *near field* $kr << 1$ and *far field* $kr >> 1$ were discussed. An effective boundary between these two regions occurs at $kr = 1$, representing a very useful guide. On the $kr < 1$ side kinetic energy (KE) began to exceed potential energy (PE), with difference growing as kr decreased further. Another hallmark of the $kr < 1$ region was that specific acoustic impedance began to go as $-i\omega\rho_0 r$ where r is distance from source, such that the basic property of sound in the form of a sound speed c, was lost. (Check out the discussion in Lecture 4.) Finally, the acoustic field components, pressure and velocity begin to become 90° out of phase in this region (see Eq.(2) of Lecture 4 to understand how this can happen.)

At this stage of game it's best to use a more precise language and call the region $kr << 1$ as the *hydrodynamic near field* (Fahy,2001) because here the fluid velocity properties are more similar to hydrodynamic flows, where compression-induced potential energy (characterized by sound speed c) is small relative to kinetic energy. The handy guide for when this happens, $kr < 1$ is still valid.

The hydrodynamic near field has range r from the source as the only length scale, which is parameterized by kr. In the current discussion involving the Rayleigh integral and beam patterns, length scales of the radiating aperture such as length L and width W, or diameter D, and properties of the acoustic field will depend on both these length scales as well as the range scale r. There is need for new definitions, defined subsequently, which will be known formally as the *geometric near field* and *geometric far field*.

With the above introduction in mind, we continue with discussion of the problem of radiation from a disk of diameter 2 m (Fig. 4). Results (Fig. 5) show calculation at 3 ranges defined by the field point $|\vec{r} - \vec{r}_s|$ equal to 4, 10 and 20 m but with varying θ. Notice that the 10 and 20 m results are quite similar (if not effectively the same) whereas results at 4 m look different. This is because 10 m and beyond represents the Fraunhofer zone (far field) for this situation defined by acoustic frequency (3000 Hz), medium speed (water 1500 m/s) and radiating aperture size (disk diameter 2

m). Observe also for the case of 10 and 20 m, that the first maximum beyond the main lobe is about 17 dB less than the main lobe of the beam, which is a far field characteristic for all beam pattern circular disk sound sources, or piston-like sources operating underwater. At range 4 m, however, the situation is quite different, because 4 m represents is still within the *geometric near field*. Notice at 4 m $kr \sim 50$ at frequency 3000 Hz, and so this range is considerably beyond the range $kr = 1$.

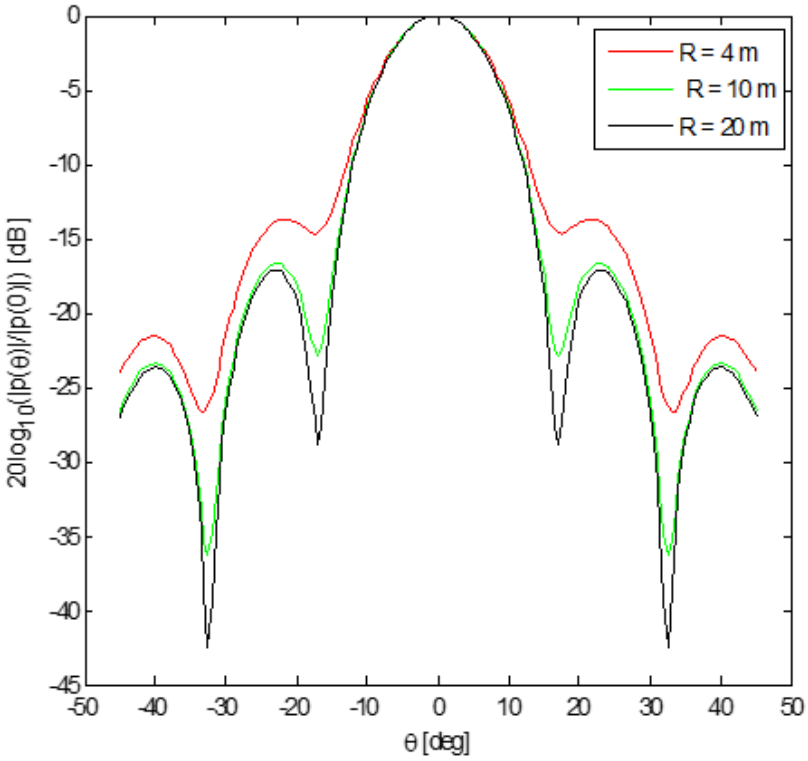

Figure 5: Results from Eq.(3) calculated at 3 ranges defined by the field point $|\vec{r} - \vec{r}_s|$ equal to 4, 10 and 20 m but with varying θ.

Another way of looking at beam patterns is a polar plot (Fig. 6) which is same as Fig. 1 of *High Frequency Underwater Sound* (which you can upload from the resource tab on the class website) representing a 43 mm diameter disk (called a piston source) with frequency 108 kHz, operating in water. Although the length and frequency scales are very different from the problem just described, observe the first side lobe is also about 17 dB less than the main lobe. Important reminder: here we are using the decibel as comparative metric. Thus we would not write " dB ref. 20μPa (for air), or ref. 1μPa (for water)".

A simple formula $\pi D^2/4\lambda$ defines the critical range where geometric far field (also called the Fraunhofer zone) behavior is expected. For any radiator of characteristic length scale L this formula is L^2/λ. For the case studied this range is ~ 6 m, which explains why the 4 m in Fig. 5 result was in the geometric near field and looked different.

Another handy formula is the beam width of the main lobe for disk transducer. This is the

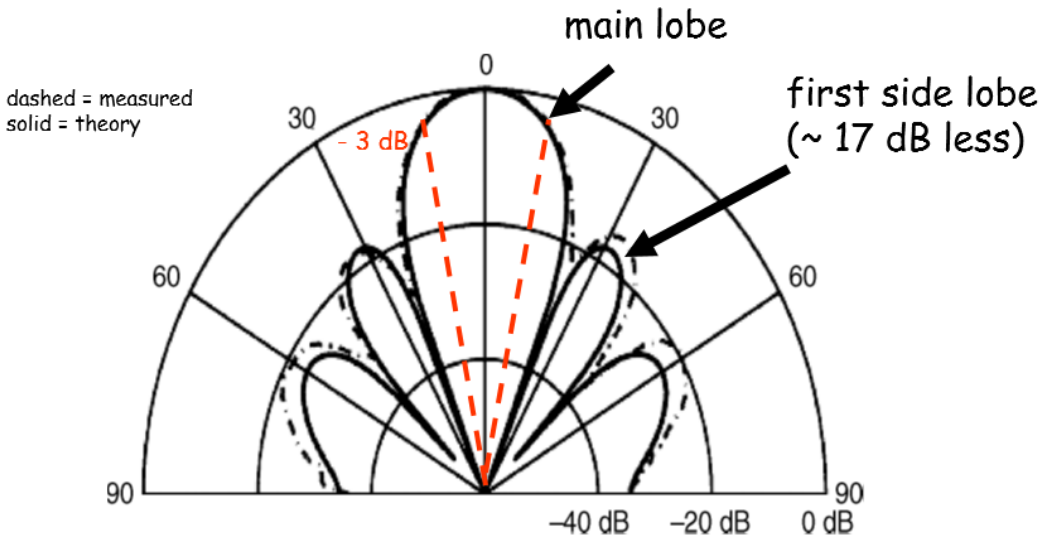

Figure 6: Polar plot of a beam pattern. See also Fig. 1 of High Frequency Underwater Sound.

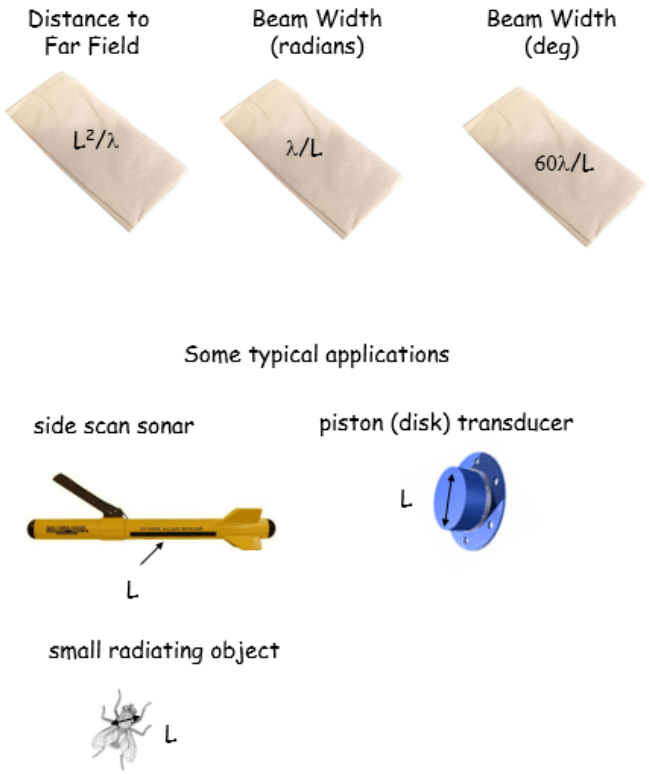

Figure 7: Some basic rules for the distance to the far field and associated beam width of a radiating aperture of length scale L and wavelength λ.

angular width represented by the red, dashed line in Fig. 6, as determined by the angle where the beam pattern has fallen by 3 dB from the maximum (sometimes called the "3 dB" width). This width (in degrees) is $60\lambda/D$ For the example of the 2 m diameter disk the formula gives $15°$.

We can summarize these handy formulas below on party napkins (impress your friends at a

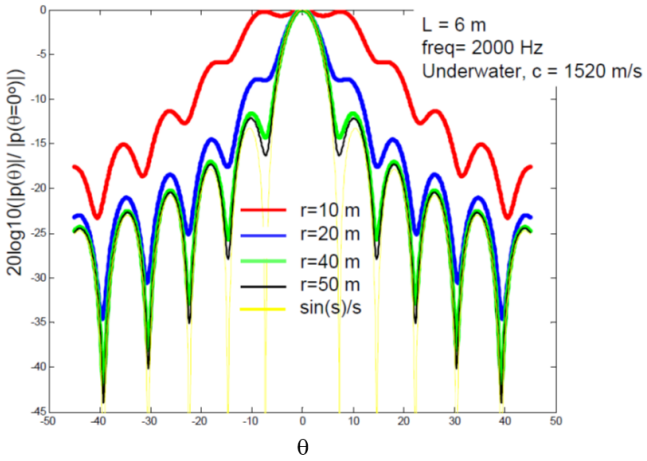

Figure 8: Beam pattern at various ranges from a line array of length 6 m operating in water at frequency 2000 Hz.

party). We use L for characteristic scale; for a disk, substitute diameter D for L and the result is nearly exact. Also, further simplify the geometric far field result by noting $\pi/4$ is sufficiently close to 1.

These are valuable for their quick-estimating power–but they can also serve as a check on any numerical study you might embark on – if the result of the study is at variance with these rules you have reason to question the results. An example involving a line array of length L (Fig. 8) shows the beam pattern evolving with range. For this case L^2/λ is about 47 m, and observe that between 40 and 50 m the beam pattern stabilizes to its geometric far field result. The far field result is $\sin(s)/s$ where $s = \frac{kL}{2}\sin(\theta)$.

Finally, exercise some caution when using this terminology. You might come across to others as being overly particular in using terms like geometric near and far field, when perhaps more experienced professionals might abbreviate these terms as near and far field while discussing beam patterns and other properties of sound radiation. One solution is to reserve the term *hydrodynamic near field* for the special case of $kr <$ and otherwise there are no length scales such as L, W or D involved, and use *near* and *far field* when such scales are involved.

References

M. C. Junger and D. Feit,*Sound, Structures, and Their Interaction* (Acoustical Society of America, and American Institute of Physics, 1993)

Pierce, A. B, *Acoustics, An Introduction to its Physical Principals and Applications*, (Acoustical Society of America, and American Institute of Physics, 1989). See in particular pp. 213-214.

F. Fahy, *Foundations of Engineering Acoustics* (Elsevier Academic Press, San Diego, CA, 2001)

ME525 Applied Acoustics Lecture 14, Winter 2022
The Rayleigh integral, additional numerical details and study of near field far field ranges

Peter H. Dahl, University of Washington

Numerical implementation of the Rayleigh Integral

A typical example for the Rayleigh integral in Eq. (1) is shown in Fig. 1

$$p(\vec{r}) = \frac{-i\omega\rho_0}{2\pi}\int_S u_n(x_s, y_s)\frac{e^{ikR}}{R}dx_s dy_s \tag{1}$$

where $R = |\vec{r} - \vec{r}_s|$. With few exceptions this is implemented numerically, the most common method through a summation from each contribution originating from area dS.[1] It is essential to properly size the elemental area dS, otherwise there will numerical errors in approximating the Rayleigh integral. From our previous notion of a monopole source of radiation area A, we anticipate a requirement that $\sqrt{dS} << \lambda$.

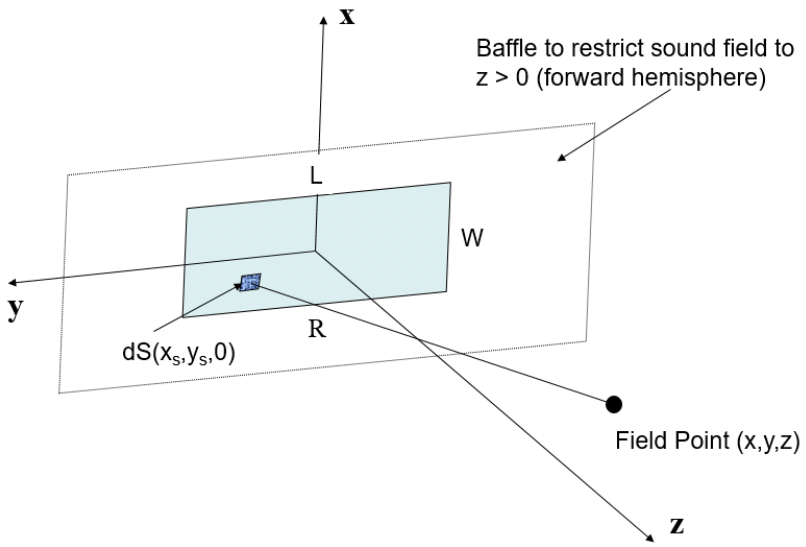

Figure 1: Cartesian coordinate system established at the center of radiating rectangular aperture confined to a baffle to restrict the sound field to $z > 0$. The elemental source dS is distance R from the field point where $R = \sqrt{(x - x_s)^2 + (y - y_s)^2 + z^2}$

It's useful to compare numerical results with an exact solution for the beam pattern of a line array in the geometric far field (this being $\sin(s)/s$ where $s = \frac{kL}{2}\sin(\theta)$). Figure 2 shows $B(\theta)$ for

[1] The term for this is a Riemann summation; see Foote,(2014).

a line array of $L = 2$ m, operating at 5000 Hz in water. This is a 1D integral so here the dS is effectively determined by dy_s, and the "length scale" of an elemental source is dy_s.

Three attempts are made as parameterized by kdy_s, and it should be clear that we need to have $kdy_s < 1$ to get acceptable results. For the case of $kdy_s = 0.21$ there is effectively no difference between the numerical and exact result. The experiment is repeated at higher frequency 8000 Hz (Fig. 3) giving a different set of three kdy_s values, showing that $kdy_s = 0.34$ is also close. Also observe the reduced beam width for 8000 Hz, as defined by angular width of the main lobe, or alternatively, width to the first null.

In summary the results suggest this rule: $kdy_s < 0.2$ for 1D line array study, and $k\sqrt{S} \leq 0.2$ for 2D study as in Fig. 1 which is of course consistent with the original conjecture of $\sqrt{dS} << \lambda$.

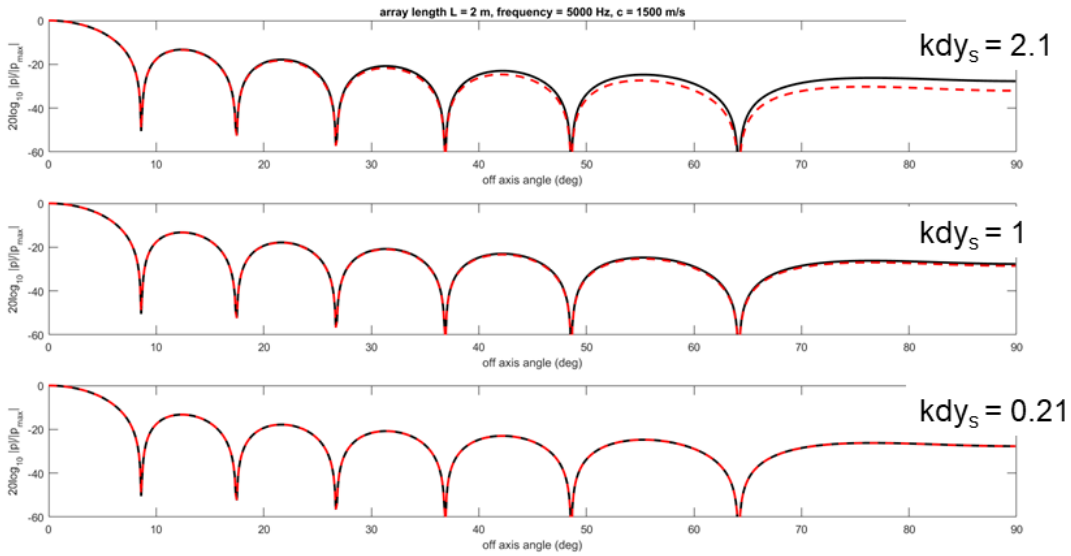

Figure 2: beam pattern $B(\theta)$ as expressed by $20\log_{10}|p(\theta)|/|p_{max}|$ computed in the far field of a line array of length 2 m, frequency 5000 Hz in water. Dashed, red line is the result computed using the identified kdy_s giving size of dy_s and solid, black line is theoretical result.

Range dependence and the near and far fields

The field on the acoustic axis of a rectangular array of $L = 1.5$ m, $W = 2$ m, is plotted as a

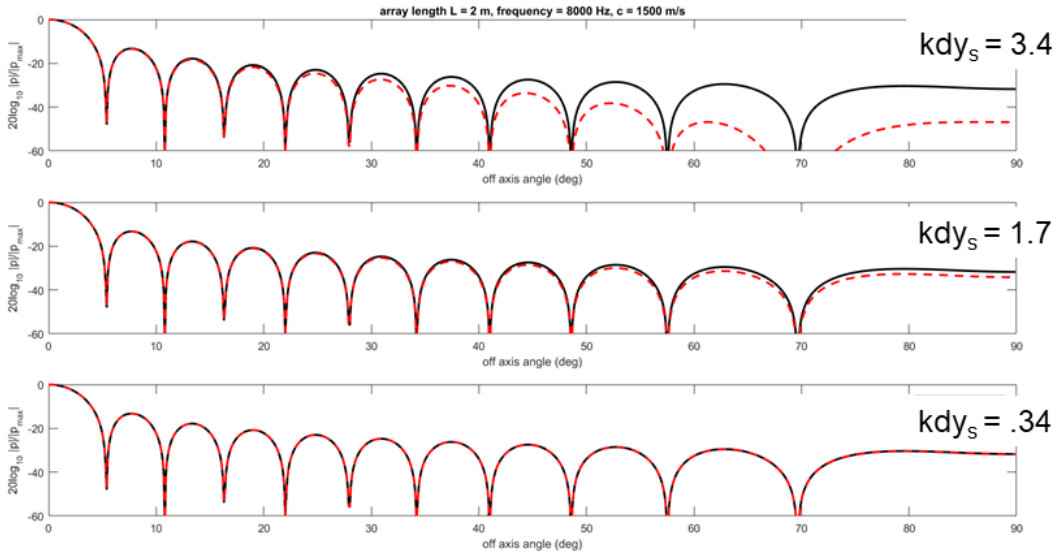

Figure 3: Beam pattern $B(\theta)$ as expressed by $20\log_{10}|p(\theta)|/|p_{max}|$ computed in the far field of a line array of length 2 m, frequency 8000 Hz in water. Dashed, red line is the result computed using the identified kdy_s giving size of dy_s and solid, black line is theoretical result.

function of range (Fig. 4), showing the complicated pattern that develops immediately in front of the array: this is the *near field*. With increasing range away from the aperature the field settles down into more smooth decay: this is the *far field*. Here pressure goes as $\sim 1/R$–or the inverse range spreading we would have expected all along from a compact point source.

The near field-far field transition is well predicted by the basic guide LW/λ. For nearly all applications, this transition must be well understood. For example, in a system calibration of this array it is desirable to place a test acoustic source (or acoustic receiver) in the far field to either receive from or transmit signals to this array. Thus, it is essential to know, with confidence, that this position is indeed in the far field because here the pressure field has simplified behavior, going as $\sim 1/R$ (dotted line in Fig. 4), and it is straightforward to correct measurement made at different ranges.

Next let us examine the 2D angular properties in the acoustic field, here using a rectangular array of $L = 1.2$ m, $W = 0.6$ m, again operating at 5000 Hz in water (Fig. 5). These calculations are

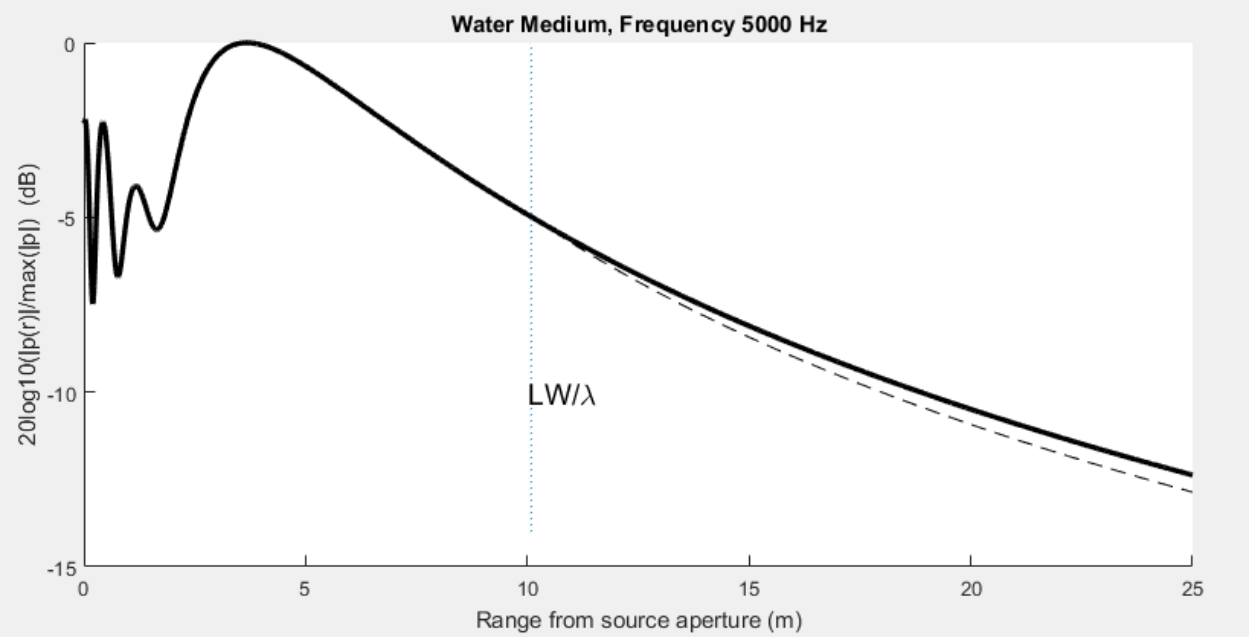

Figure 4: Relative magnitude of pressure field (expressed dB) on the acoustic axis of a rectangular array of array of $L = 1.5$ m, $W = 2$ m as function of range, for frequency 5000 Hz operating in water. The near-far field transition point is shown at range = LW/λ, after the pressure magnitude goes as $\sim 1/R$

made well into the far field (i.e., range $>> LW/\lambda$), and you should by now have an intuitive feel for the results.

With reference to Fig. 1, for one case in Fig. 5, θ sweeps across the L dimension such that $\theta = 0^\circ$ aligns with z axis and $\theta = 90^\circ$ aligns with y axis; for the other case θ sweeps across the W dimension such that $\theta = 90^\circ$ aligns with x axis. Since $L > W$ we expect the beam width across L to be more narrow than that across the W dimension, consistent with the Fourier relation between aperture scale and angular width. Since the calculations are made well in the far field the $\sin(s)/s$ associated with each dimension predicts the beam pattern quite well, where s is either $\frac{kL}{2}\sin(\theta))$ or $\frac{kW}{2}\sin(\theta)$. Figure 6 shows the beam pattern as if looking straight into the beam at some position in far field. Because the long side L is oriented horizontally, the beam appears more narrow in this direction.

Array shading and a practical application of the Rayleigh Integral in Medical Ultrasound

A simple demonstration of aperture (or array) shading is illustrated in Fig. 7. An aperture about 15 by 21 cm is shown on the left side. The unshaded narrow beam based on the full 15 by 21 cm dimension is shown by the red beam pattern on the right side. We can shade this aperture in a simple way by by setting all sources, as in $u_n(x_s, y_s)$ of Eq.(1), to 0, for source locations on the corners of the aperture. The shaded aperture is shown by the black on left side and corresponding beam pattern on right side. The total length of the shaded aperture is still the same but you can see that the shaded beam pattern has broadened somewhat and side lobes have been reduced.

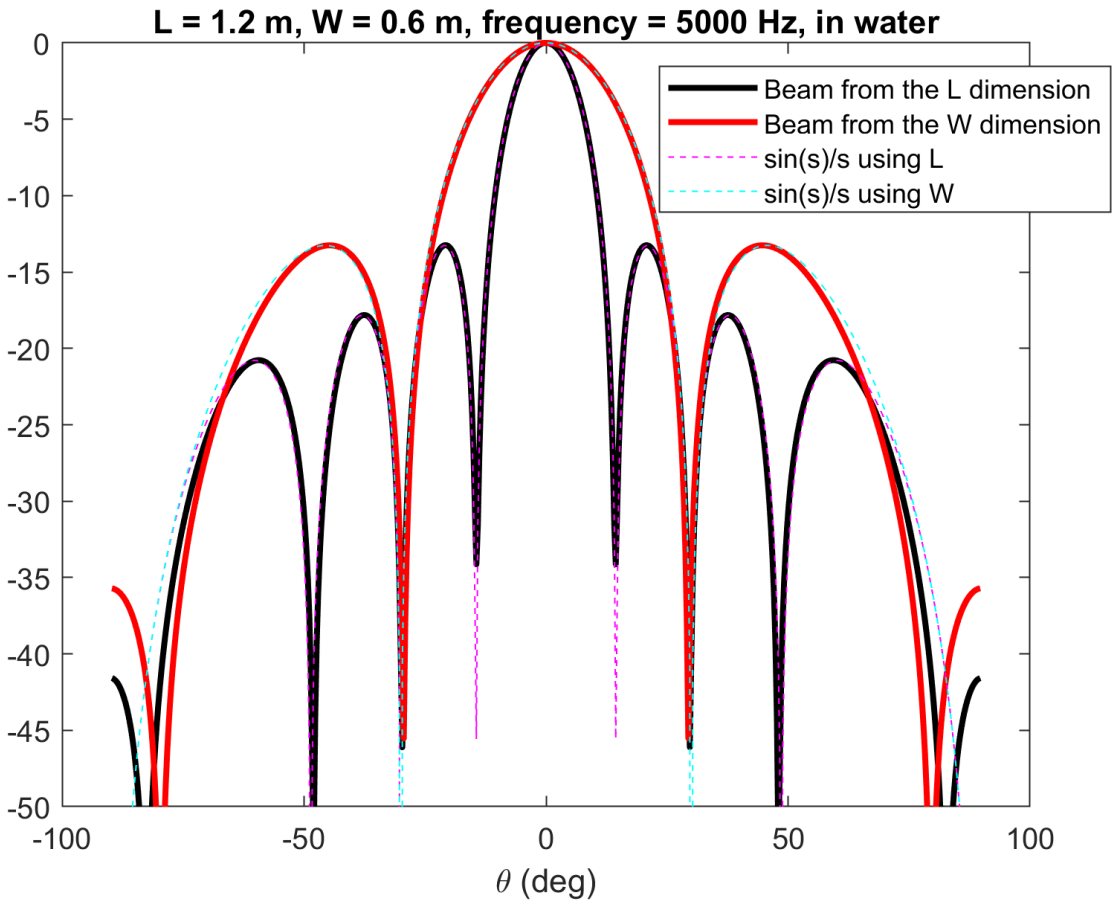

Figure 5: Relative magnitude of pressure field (expressed dB) on the acoustic axis of a rectangular array of array of $L = 1.2$ m, $W = 0.6$ m as function of angle θ, for frequency 5000 Hz operating in water. For one case θ sweeps across the L dimension such that $\theta = 0°$ aligns with z axis and $\theta = 90°$ aligns with y axis; for the other case θ sweeps across the W dimension such that $\theta = 90°$ aligns with x axis. See Fig. 1 for geometry.

There are many applications where this result is desirable and the Rayleigh integral can be used as an exploratory tool find an optimal solution. A more sophisticated example of this is provided by Dr. Wayne Kreider of the Applied Physics Laboratory's Center for Industrial and Medical Ultrasound. In this case the aperture is composed of 256 elements arranged in a spiral (Fig. 8) which at the transmit frequency of 1.5 MHz, produces a focus point at about 120 mm away on the acoustic axis (Fig. 9). Keep in mind that given the combination of element diameter d of 7 mm, and the high frequency 1.5 MHz, puts $kd >> 1$ and thus a Riemann summation with appropriately small dS must be applied to each of the 256 elements. More on this study can be found in Kreider, *et al.* (2018).

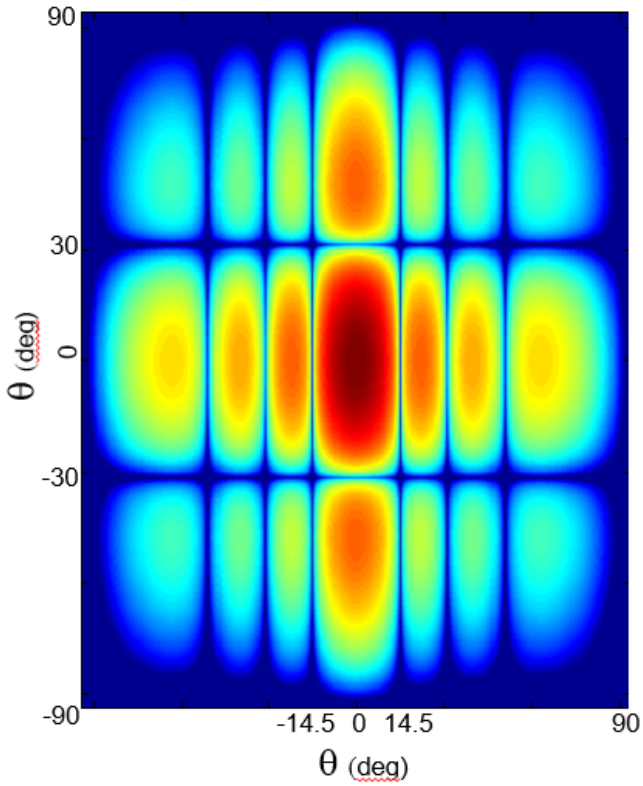

Figure 6: Beam pattern from example in Fig. 5 as if looking straight into the beam at some position in far field. Red-to-blue denotes high-to-low levels of the beam pattern. The beam originates from an aperture shown in Fig. 1. Because the long side L is oriented horizontally, the beam appears more narrow in this direction.

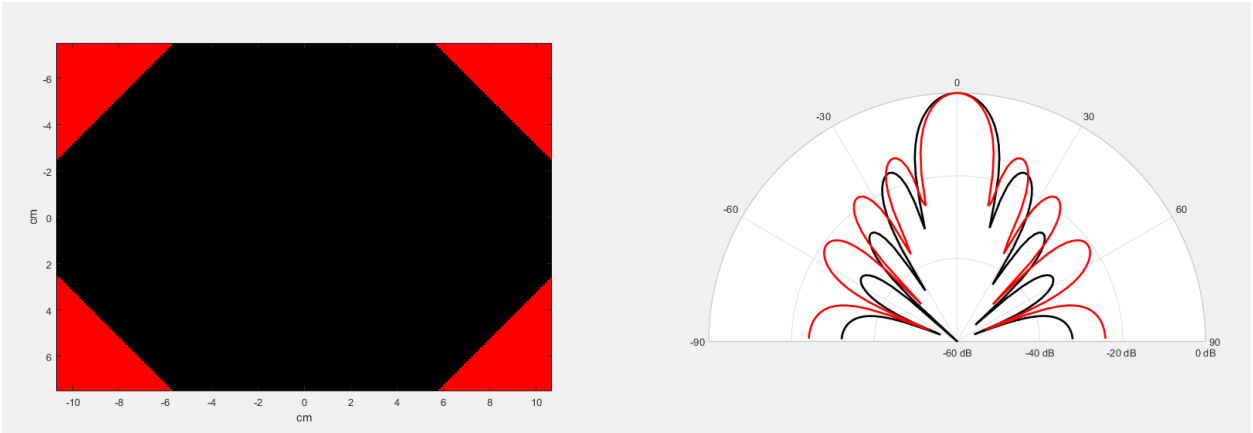

Figure 7: left side: shaded aperture (black) and unshaded aperture (red + black). Right side: Beam pattern computed in the far field for frequency 30 kHz, representing pattern for the long axis of the aperture, for shaded aperture (black) and unshaded aperture (red).

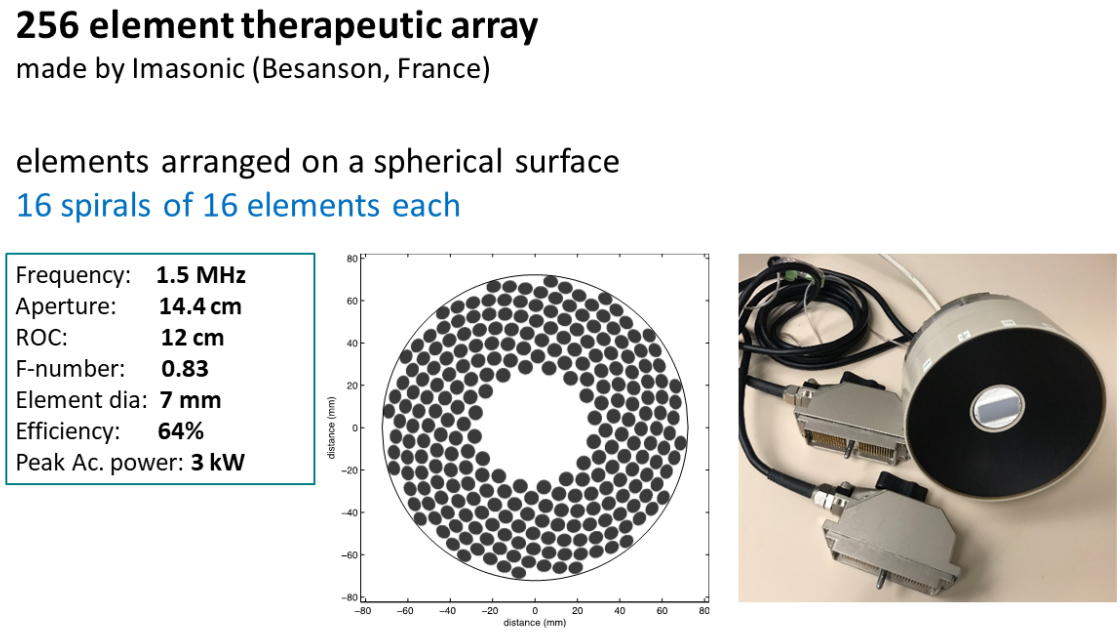

Figure 8: 256 element spiral array used for focused ultrasound applications in diagnostic and therapeutic applications in medical ultrasound.

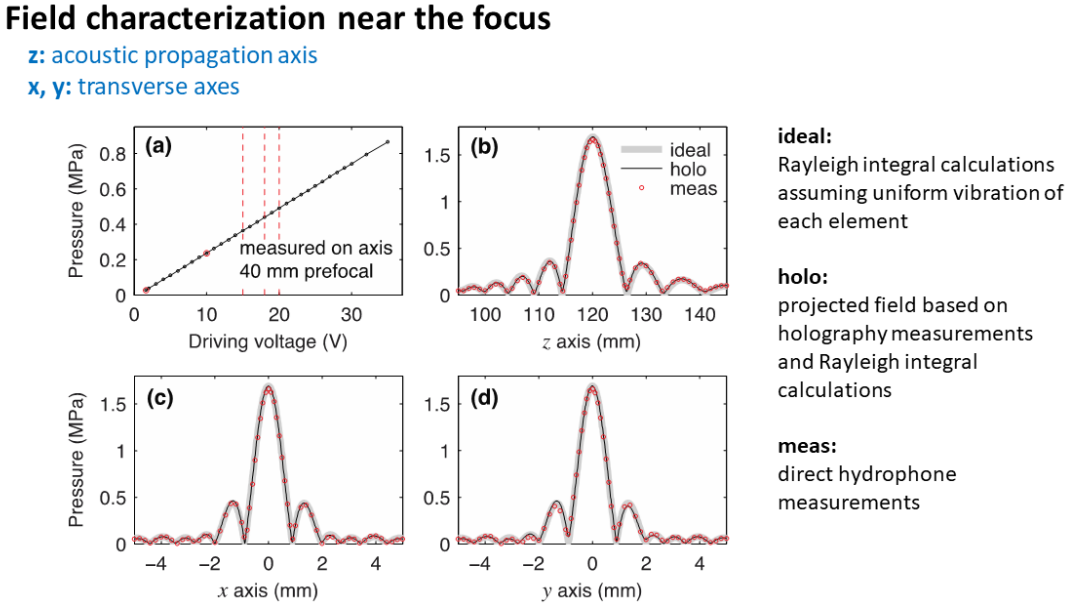

Figure 9: Field characterization near the focus points based on the Rayleigh integral (thick, gray lines) compared with measurement.

References

K.G. Foote , "Discriminating between the nearfield and the farfield of acoustic transducers," *J. Acoust. Soc. Am.* 136, October 2014.

W. Kreider *et al.*, "Characterization of Multi-Element Clinical HIFU System Using Acoustic Holography and Non-linear Modeling," *IEEE Transactions on Ultrasonics, Ferroelectrics, and Frequency Control* 60, August 2018.